Seismic and geologic controls on spatial clustering of landslides in three large earthquakes

Claire Rault[1], Alexandra Robert[2], Odin Marc[3], Niels Hovius[4, 5], Patrick Meunier[1]

[1] Laboratoire de Géologie, Ecole Normale Supérieure Paris, Paris, 75005, France
[2] Géosciences Environnement Toulouse, Observatoire Midi-Pyrénées, Toulouse, 31400, France
[3] Ecole et Observatoire des Sciences de la Terre, Strasbourg, 67084, France
[4] GFZ German Research Center for Geosciences, Potsdam, 14473, Germany
[5] Institute for Earth and Environmental Sciences, University of Potsdam, 14476, Germany

Correspondence to: Claire Rault (claire.rault@ens.fr)

Abstract. The large, shallow earthquakes at Northridge, California (1994), Chi-Chi, Taiwan (1999) and Wenchuan, China (2008) each triggered thousands of landslides. We have determined the position of these landslides along hillslopes, normalizing for statistical bias. The landslide patterns have a co-seismic signature, with clustering at ridge crests and slope toes. A cross check against rainfall-induced landslide inventories seems to confirm that crest-clustering is specific to seismic-triggering as observed in previous studies. In our three study areas, the seismic ground motion parameters, lithologic and topographic features used do not seem to exert a primary control on the observed patterns of landslide clustering. However, we show that at the scale of the epicentral area, crest- and toe-clustering occur in areas with specific geological features. Toe-clustering of seismically-induced landslides tends to occur along regional major faults. Crest-clustering is concentrated at sites where the lithology along hillslopes is approximately uniform, or made of alternating soft and hard strata, and without strong overprint of geological structures. Although earthquake-induced landslides locate higher on hillslopes in a statistically significant way, geological features strongly modulate the landslide position along the hillslopes. As a result the observation of landslide clustering on topographic ridges cannot be used as a definite indicator of topographic amplification of ground shaking.

1 Introduction

Seismic ground shaking triggers many landslides in active mountain areas. A growing number of catalogues of landslides associated with large earthquakes is now being produced by mapping from satellite images (Tanyaş et al., 2017; U.S. Geological Survey, 2018b). Such catalogues have been used to show that to the first order, the density of the co-seismic landslides is controlled by the intensity of seismic shaking and by hillslope rock strength, and that the total volume of landslides and the area extent affected by them increase with the earthquake magnitude (Keefer, 1984; Marc et al., 2016, 2017; Rodríguez et al., 1999).

In recent years, several studies have explored the position of the landslides in the landscape, adding this characteristic to their description of the landslide inventories. At the catchment scale, landslides triggered by storms and earthquakes affect different parts of ridge and valley topography (Densmore and Hovius, 2000; Meunier et al., 2008). Storm-induced landslides are preferentially triggered low on slopes due to riverbank erosion and high groundwater pressure (Lin et al., 2011; Meunier et al., 2008; Tseng et al., 2017). By contrast, earthquake-triggered landslides are more uniformly distributed since ground shaking affects all portions of the hillslope (Densmore and Hovius, 2000), or they are concentrated near ridges or slope breaks (Harp and Jibson, 1996; Massey et al., 2017; Sepúlveda et al., 2010; Weissel and Stark, 2001). Numerical simulations of ground shaking in complex topographies predict that seismic waves are actually amplified around ridge crests (e.g. Boore, 1973; Massa et al., 2014; Poursartip et al., 2017). Both seismic noise analysis and strong motion records confirm that stronger shaking often occurs at topographic highs (Chávez-García et al., 1996; Durante et al., 2017; Hartzell et al., 2014; Massa et al., 2010). Meunier et al, 2008 suggested that earthquake-induced landslides tend to cluster around ridge crests as a consequence of these topographic site effects. Yet, amplification of ground shaking around the crests predicted by numerical studies is found to be modest, mostly 1.2 to 2.5 times the flat model, depending in particular on the shape of the hill and the seismic wave frequency considered (Ashford et al., 1997; Asimaki and Mohammadi, 2018; Chávez-García et al., 1996; Geli et al., 1988; Lovati et al., 2011; Pedersen et al., 1994). Numerous authors argued that larger crest amplifications observed in the field are mostly caused by lithological contrasts along the wave path and possible upward propagation of Rayleigh waves from the base of a slope towards the crest (Burjánek et al., 2014; Gallipoli et al., 2013; Glinsky and Bertrand, 2017; Havenith et al., 2003; Ohtsuki and Harumi, 1983).

Here, we study the spatial variations of the position of co-seismic landslides on hillslopes within the epicentral areas of three large, shallow earthquakes affecting steep mountain topography: the 1994 M_w 6.7 Northridge Earthquake, the 1999 M_w 7.6 Chi-Chi Earthquake and the 2008 M_w 7.9 Wenchuan Earthquake. We also consider the location of rainfall-triggered landslides in the area affected by the Chi-Chi earthquake for comparison. Using a statistical approach, we identify coherent patterns of ridge crest- and slope toe-clustering. We explore seismic, topographic, lithological and structural features as possible controls on the observed patterns, and conclude that co-seismic landslide distributions are best explained by superposition of effects of local geological configurations on general seismically-controlled patterns.

2 Study areas and landslides inventories

We use previously published landslides inventories for three earthquakes (Table 1), constructed by digitizing landslides outlines from field and air-photos, and satellites images. These inventories have been shown to be relatively complete for landslides larger than 30 m^2, but they do not allow distinction between the erosional and depositional parts of landslides.

2.1 The 1994 Northridge earthquake

The M_w 6.7 Northridge occurred on the 17th of January 1994, about 100km North of Los Angeles, in Southern California. Rupture started on the Northridge blind thrust fault, at about 19km depth (Somerville et al., 1996). It generated strong ground shaking with peak ground accelerations (PGA) up to 1.78g. More than 11.000 landslides were triggered, with a cumulative area of more than 23km^2 (Harp and Jibson, 1996). Most of these landslides were located in the Santa Susanna and San Gabriel Mountains.

2.2 The 1999 Chi-Chi earthquake

On the 21st September 1999, the shallow M_w 7.6 Chi-Chi earthquake occurred in the western foothills of Taiwan's Central Range. The rupture initiated along the Chelungpu thrust fault at 12±5km depth (Angelier et al., 2001). Strong ground shaking was recorded with a PGA up to 1g in some places (Tsai et al, 2000). The earthquake caused about 10,000 landslides with a combined area in excess of 125 km^2 (Liao and Lee, 2000).

2.3 The 2008 Wenchuan earthquake

On the 12th of May 2008, the M_w 7.9 Wenchuan earthquake occurred along the eastern boundary of the Tibetan Plateau. The rupture initiated at a focal depth of 14 to 19km and propagated along two segments of the Longmen Shan thrust system (De Michele et al., 2010; Tong et al., 2010). Strong ground motion was felt with recorded PGA exceeding 0.8g in some places (Wen et al., 2010) . The earthquake caused a large number of landslides: more than 197,000 were mapped, with a cumulative surface area exceeding 700km² (Xu et al., 2014). At least three catalogues are available for this earthquake (Gorum et al., 2011; Parker et al., 2011; Xu et al., 2014). Here, we use the one from Xu et al 2014, which we deem to be the most complete and accurate, based on a comparison detailed in the supplementary materials.

2.4 Rainfall-induced landslides in the Chi-Chi epicentral area

In 2009, typhoon Morakot deposited up to 31.9 meter of rainwater in 48 hours in the considered area (Chien and Kuo, 2011). More than 15,000 landslides were triggered by this typhoon (Marc et al., 2018) in an area that extends into the Chi-Chi epicentral area. In the area of overlap, the characteristics of the landslide populations associated with the earthquake and the typhoon can be compared directly. Moreover, we document the time variation of the location of the landslides located in three watersheds in the Chi-Chi epicentral area from 1994 to 2014 (Marc et al., 2015, Table 1). The location of these three catchments is reported in Fig. 2 and 3.

3 Methods

3.1 Landslide position in the landscape

Our aim is to determine the position of landslides within the landscape, specifically their position relative to a ridge crest or the top of a hillslope, and to the river valley or toe of a hillslope. For this, we adopt the metrics of Meunier et al, 2008 to normalize for the variation of hillslope lengths across the landscape, introducing the normalized distance to stream $|d_{st}|$. Ridge crests are characterized by a $|d_{st}|$ equal to one, while rivers have a $|d_{st}|$ equal to zero (see supplementary, Method and metrics).

A given portion of the landscape is characterized by its probability density function of occurrence of $|d_{st}|$ values, PDF_{topo} (Fig. S1.e). Landslide locations are characterized by PDF_{ls}, the probability density function of $|dst|$ derived only from cells affected by landslides. Within portions of the epicentral area (macrocells), we compute both PDF_{topo} and PDF_{ls} and we define the ratio of probability $R_p= PDF_{ls}/PDF_{topo}$. In this way, the distribution of locations of the landsliding cells along hillslopes (here expressed in $|d_{st}|$) is normalized by the distribution of occurrence of locations in the landscape of the macrocell, effectively removing geomorphic or methodological biases (Fig. S1.e, S1.f). If the landscape into the macrocell is uniformly sampled by landsliding, $R_p=1$ over (0,1). High values of R_p (>>1) for $|d_{st}|$ >0.75 indicate a significant crest oversampling by landslides. Inversely, low values of R_p express undersampling. Similarly, large values of R_p for $|d_{st}|$<0.25 indicate hillslope toe oversampling. In our analysis, we have defined $Rp_{crest} = \overline{Rp_{[0.75-1)}}$ and $Rp_{toe} = \overline{Rp_{(0-0.25]}}$ as the mean value of R_p over the upper and the lower quarter of the hillslope respectively.

3.2 Crest and toe clustering

The purpose of this paper is first to detect if there are areas where the landslides are more likely to occur on a given portion of the hillslope (i.e. if crests or toes are more susceptible to fail during an earthquakes), and if so, what physical processes could explain it. Macrocells with very few landslides are not statistically representative. Therefore, we must be able to quantify the probability for a given topography and landslides within it that the observed R_p could differ from one because of statistical fluctuations rather than for physical reasons. To do this, we test the null hypothesis comparing the R_p derived from the data to the one associated to a random sampling of the landscape. In each macrocell, we define the 90% interval of confidence I_{rp} depending on the number of landslides affecting it. Crest-clustering, defined here as preferential sampling of the upper quarter of a hillslope section by landsliding, is only considered to occur where Rp_{crest} exceeds the upper bound of I_{rp}. Similarly, Rp_{toe} is defined as the average of Rp computed over the lower quarter of the slope, and toe-clustering is adjudged for Rp_{toe} values greater than the upper-bound of I_{rp} (Fig. S2). Since crest-clustering and toe-clustering are mutually exclusive (see supplementary, Statistical robustness, Fig. S4), zones of toe-clustering also have values of Rp_{crest} lower than the lower bound of I_{rp}. Therefore, Rp_{crest} can be used as an indicator of crest- and toe-clustering.

3.3 Spatial mapping of the landslide position within the epicentral area

Maps of Rp_{crest} and Rp_{toe} were generated by subdividing a study area into macrocells in which Rp is calculated. The size of the macrocells in this study is set at 7.8 km^2 to optimize for two criteria: a) the cell must be small enough to capture the spatial variation within the epicentral area, and b) it must be large enough to be statistically representative in terms of landslide content (see supplementary Methods-Metrics). The second criterion imposes a lower limit to the resolution at which we can observe any spatial variation. Figure S5 shows three Rp_{crest} maps in the Wenchuan epicentral area with increasing macrocell size. Although the patterns remain globally the same, macrocells of 7.8 km^2 produce the most legible map. The mean of Rp_{crest}, averaged over the whole landscape, remains relatively independent of the macrocell size (Table 2, supplementary).

3.4 Extraction of seismic and topographic parameters

In each macrocell, we compute the median of the seismic parameters according to the USGS ShakeMap (Allen and Wald 2007; U.S. Geological Survey 2018a). Shake maps provide the peak ground velocity (PGV), peak ground acceleration (PGA), and the pseudo spectral acceleration (PSA) at 3s, 1s, and 0.3s.

relations have been observed between seismic ground motion and the ridge shape and orientation with respect to the epicenter. For example, the ridge half width can be related to the frequency of resonance of the topography (e.g. Paolucci, 2002, Massa et al, 2014) and the ridge shape ratio (slope height /ridge width) can be linked to the ground motion amplification (Geli, 1988). To test if the clustering can be associated to the geometry of the ridges we calculate and associate to each macrocell the median slope heights and the median of the ridge half-widths. To do this, we perform a geometric extraction of the ridge relief by simplifying the geometry of the topographic ridge cross section by a triangular shape (see supplementary extraction of topographic features Fig. S8).

3.5 Lithological features

In order constrain the influence of rock strength on landslide location patterns, we group lithologies that have similar apparent physical properties, using the information provided by geological maps of the earthquake epicentral areas (see Fig. S9). For the Northridge area, we use a combination of the maps compiled by the United States Geological Survey (Yerkes et al., 2005; Strand, 1969). For Taiwan we use materials from the Taiwan Central Geological Survey, MOEA (MOEA and Central Geological Survey, 2008), and for Wenchuan we use the map published by Robert, 2011. Each macrocell is defined by its dominant lithology group, *i.e*, the one occupying the largest area.

4 Results

4.1 Temporal variation of crest-clustering

To test if seismic ground shaking and rainstorms cause hillslope failures in different parts of the landscape, we first consider the temporal variation of clustering in the upper quartile of slopes in three watersheds in the Chi-Chi epicentral area between 1996 and 2014 (Fig. 1). Before the Chi-Chi earthquake, the typhoon-induced landslides tended to under-sample the upper slope domain ($Rp_{crest} < 0.6$). The Chi-Chi earthquake itself was characterized by clear crest over-sampling ($Rp_{crest} = 1.2$). Just after the earthquake, Rp_{crest} dropped to 0.4 and returned to its pre-earthquake value in about 3 years. This evolution seems to confirm that landslides triggered by earthquakes and rainfall have distinct and different clustering behaviour as observed in previous study (Meunier et al, 2008; Densmore and Hovius, 2000).

4.2 Spatial variation of crest-clustering

Figure 2 shows the spatial distribution of Rp_{crest} in the three epicentral areas. Macrocells without statistically significant clustering are removed for clarity (see Methods-Statistics). In the three cases, we observe coherent patterns of crest- and toe-clustering on about half of the surface affected by landsliding (Fig. 2). These patterns can cover several tens of square kilometers, and they have similar sizes in the three epicentral areas. Hence, the larger the epicentral area the more individual patterns we observe. Specifically, the Northridge epicentral area is almost exclusively affected by crest-clustering (Fig. 2.b). Two coherent zones are observed in the Chi-Chi epicentral area: crest-clustering in the western-part of the epicentral area, and toe-clustering in the eastern part (Fig. 2.c). In the Wenchuan case, five or six distinct patches of crest-clustering can be identified. They are separated by more or less elongated zones of toe-clustering extending up to several tens of kilometers (Fig. 2.a). Overall, crest-clustering does not appear to be a dominant pattern in the Wenchuan case. Note that in the Wenchuan case, the pattern of clustering is very sensitive to the quality of the landslide inventory (see dependence on the datasets in the supplementary). In the following, we only consider results obtained with the Xu et al, 2014 dataset. Therefore, the three cases show that earthquake-triggered landslides are distributed quite evenly along many slopes in an epicentral area, with upper slope or slope toe clustering in some places.

The spatial distribution of Rp_{crest} for the landslides induced by typhoon Morakot in Taiwan is distinct from that found for the three earthquakes. The typhoon caused uniform toe-clustering (Fig. 3), with lower values of Rp_{crest} (~0.5) in the aforementioned watersheds than those obtained in the same region for landslides induced by the Chi-Chi earthquake, even though these also cluster downslope. This observation, added to the results concerning the temporal variation of Rp_{crest} presented in the section 4.1, suggests that toe-clustering is a signature of rainfall-induced landslides.

5 Controls of clustering

Pervasive crest-clustering of co-seismic landslides within an earthquake epicentral area would signal predominance of seismic controls over any other controls. By contrast, a noisy distribution of crest-clustering could suggest that the location of landslides is controlled by highly variable local factors such as topographic slope, soil moisture or soil depth. The existence of coherent patterns of crest-or toe-clustering over hundreds of square kilometers suggests a large-scale control such as regional geological structures or geomorphic features.

5.1 Seismic controls

In our examples, crest-clustering is not primarily explained by regional seismic parameters. Figure 4 shows Rp_{crest} plotted against the median of Peak Ground Velocity (PGV) (Fig. 4.a) and Pseudo Static Acceleration at 1s ($PSA\ 1s$) published on ShakeMap (Fig. 4.b). For the Northridge and Wenchuan earthquakes, crest- and toe- clustering both occur over a wide range of PGV (1-100 cm/s) and PSA (0.1-1g). In Taiwan, Rp_{crest} weakly increases with PGV and PSA_{1s} but the spatial distribution of the patterns relative to the regional geological structure may cause misattribution. Indeed, as PGV and PSA strongly decrease towards the east, the strength of the geological units increases (see Sec. 5.3) (see Fig. S12). Similar results are found for PGA and PSA_{3s} (Fig. S13).

5.2 Geomorphic controls

Local hillslope geometry does not explain cluster location. Figure 5.c shows Rp_{crest} plotted against the median of the ratio of the gradient of the upper and lower hillslope quarters. No correlation can be identified. Both hillslope local relief and aspect ratio also fail to segregate zones of crest-clustering from zones of toe-clustering (Fig. 5.a-b) with possible exception of the Chi-Chi case. There Rp_{crest} seems to decrease as slopes become higher and steeper.

5.3 Geological control on Rp_{crest} distribution

Maps of Rp_{crest} projected on the main lithological units of the three epicentral areas are shown in Fig. S9. Meanwhile, the statistical distributions of Rp_{crest} per lithology are reported in boxplots in Fig. 6. In the Chi-Chi case, crest-clustering is principally observed in the western foothills that are comprising of poorly consolidated sandstones with interbedded marls and mudstones (Camanni et al., 2014; MOEA and Central Geological Survey, 2008) (Fig. 6.b. and Fig S9.c). The higher grade lithological units to the east are mainly affected by toe-clustering. Hence, lithology seems to be a first-order control on the distribution patterns of Rp_{crest}.

However, in Northidge and Wenchuan cases, the distribution of Rp_{crest} is not correlated in a simple way with rock strength according to simple lithological classes (Fig. 6.a-c). In the Wenchuan epicentral area, rocks with various deformation grades

are observed, depending among other things on the major geological structures that intersect them. For instance, intensely deformed sandstones are found into the Wenchuan Shear Zone, while they are moderately deformed within the Songpan Garze units, and relatively intact in the foothills (e.g. Robert, 2011). This geological diversity allows a more detailed, ad hoc analysis of substrate controls on landslide location.

From our data, crest- and toe-clustering of co-seismic landslides seem to be concentrated along specific geological features. This is illustrated by the following observations from the Wenchuan epicentral area, which is large and geologically diverse. In the Wenchuan shear zone, landslide toe-clustering occurs along the Minjiang river valley (Fig. 7.b). This river is entrained in the Wenchuan shear zone over more than 60km, where deformation of rocks is very intense (e.g. Godard et al., 2010; Liu-Zeng et al., 2011). In this area, mostly Paleozoic rocks have several schistosities and intense foliation that strongly decrease their strength (Fig. 7 cross section A-B). The deformation is particularly intense in this zone due to the presence of resistant granitic massifs on both side of the fault zone (Robert, 2011). The most weakened material is downslope where the fault cuts the surface.

The central part of the foothills of the Longmen Shan is characterized by two large units: the so-called "upper unit" has large lithological contrasts over short distances (~10km) due to folding and thrusting, while the "lower unit" is more uniform (Fig. 7.a-c cross section C-D). In the upper unit co-seismic landslides have a coherent toe-clustering pattern, whereas the lower unit has a clear crest-clustering pattern (Fig. 7.a and S14.b). A strong concentration of landslides is observed on lower slope segments along the Beichuan fault, especially up to the Jinhe and Mianyuan rivers branches (Fig. 7 and S14.b). Around this fault, massive Permian dolomites top the cataclastic Triassic rocks, which crop out along the Tuojiang river, forcing failures downslope. In the area of Qiaping, between the Beichuan fault and the Pengguan massif and along the Mianyuan river, the Silurian and Devonian sedimentary rock layers are dipping steeply and bear traces of strong deformation, including pervasive schistosity. (Robert, 2011) (Fig. 7.a-c cross section E-F). There, the downslope layers could be more susceptible to toppling onto the riverbed. The location of landslides is thus strongly controlled by the stratigraphy (weak rocks downslope topped by strong rock forming the crests), bedding dip, and the fault weakening zone.

In the foothills of the Longmen Shan, except the central part discussed above, crest-clustering of landslides is clearly dominant. In the north-eastern part, most of the landslides oversampled the crests of the large Tangwanzhai syncline (Fig. 7 and S17.d). In this area, the presence of this large syncline strongly influences the morphology as the crests formed by sandstone and limestone strata are almost parallel to the Wenchuan fault system (Fig. 7.a and c cross section G-H and Fig. S15 cross section I-J). Similar patterns are observed in the Sanjiang klippe and on both sides of the Tuojiang river, in the Longmen Shan Central Zone (Fig. 7, S14.a and S15 cross section K-L). These crests are made of stronger and more resistant rocks implying the formation of steep slopes in the direction opposite to the dip of sedimentary layering. This slope asymmetry is marked by a strong curvature along the crests, a configuration that could favour amplification of ground-motion promoting toppling or wedge failures.

Finally, in earthquake affected Crystalline Massifs of the Longmen Shan (Pengguan, Xuelang Bao and Baoxing), crest-clustering is also dominant, except along the Minjiang river (Fig. 7.a).

Meanwhile, in the Chi-Chi epicentral area, crest-clustering is observed in the foothills made of terrace deposits and alternating of sandstone and shale strata (Fig. S7.c). Toe-clustering is found in the eastern part of the epicentral area where steep valleys and important fault system are cutting the shaly sandstones and slightly metamorphosed argilite layers (Fig. S9.c).

In the Northridge area, crest-clustering is observed where interbedded conglomerate sandstones and shales form the crests of the Northern part of the Santa Susanna Mountains (Harp and Jibson, 1996; Winterer and Durham, 1962) (Fig. S16). There, co-seismic landslides preferentially occurred on the top of the scarp slopes. This configuration seems to be similar to that in the Tangwanzhai area of the Wenchuan earthquake (Fig S17.d) Crest-clustering is also observed in the so called badlands at the fringe of the Santa Clarita basin which have formed in a homogeneous weak lithology (Fig. S9.b).

In summary, three main types of geological effects were identified as major controls on landslide clustering: a) rivers flowing along fault zones with structurally weakened rocks, b) stratigraphic alternations of strong and weak units and c) the effect of the bedding on very steep hillslopes.

6 Discussion and conclusion

In this study we have systematically tested for a range of controls on the position of co-seismic landslides relative to the toe and the crest of hillslopes. Confirming previous studies (*e.g.* Densmore and Hovius, 2000, Meunier et al., 2008), we find that rain-triggered landslides occur preferentially at slope toes, likely due to high pore pressures associated with infiltration and fast downslope flow of groundwater in fractured rock mass, regolith and colluvium during rainfall. The location of earthquake-triggered landslides is, on average, higher on hillslopes than the rainfall-induced one, and displays coherent patterns of toe-and-crest clustering spread all over the epicentral area. Where we have identified clear patterns of crest- and toe-clustering within the epicentral area of Northridge, Chi-Chi, and Wenchuan earthquakes, these are due to a combination of seismic mechanisms and geological controls.

Toe-clustering of seismically-triggered landslides occurs mainly in areas where hillslope materials are heavily fractured, weathered, particularly in river valleys along major fault zones, and more specifically near the fault where the deformation is the highest. The influence of fault zone weakening on slope stability have been documented in other contexts (e.g. Demir et al., 2013; Korup, 2004; Scheingross et al., 2013). In absence of particular geological structures toe-clustering is also observed along trunk valleys in hard rock massifs where static stress can have induced severe fracturing at the base of topographic ridges (Molnar, 2004), and where weak stratigraphic units crop out low in mountain landscapes. Therefore toe-clustering of co-seismic landslides appears to be explained at the first order by geological and structural controls. These controls add to any effects of possible downslope seismic amplification due to surface wave generation or directional effects (Pilz et al., 2018; Wasowski et al., 2013).

Crest-clustering of co-seismic landslides is found primarily in areas without strong lithological contrasts, specific geological structures or away from river trunk valleys. It is particularly well developed in regions underlain by sedimentary rocks,

where ridge crests are defined by specific beds oriented parallel to the seismogenic faults. In these particular geological configurations, topographic amplification could control the landslide position. For example, in the Tangwanzhai syncline, the sharpest crests are oversampled by landslides (see supplementary topographic amplification, Fig. S17). Several authors have shown that ridge sharpness promotes topographic amplification (Maufroy et al., 2015; Rai et al., 2016). The landslide position would thus reflect of the expression of strong ground motion in the uppermost part of the slope which can be explained by complex interactions of various seismic waves with both topography and lithology. The focusing of waves on the edges of slopes may induce sufficient amplification of the ground motion to trigger slope failures (e.g Kaiser et al., 2013; Stahl et al., 2014). Higher levels of amplification may be reached when the incoming wave is perpendicular to the ridge elongation (Massa et al., 2010), and thus increase the probability of failure. Moreover some authors suggest that Rayleigh waves, generated at the toe of the hillslope and propagating toward the ridge-crest, would produce an added inertial force on the sliding mass and increase the duration of ground motion, favoring upper slope failures (Jafarzadeh et al., 2015; Poursartip and Kallivokas, 2018).

We do not find clear explanations for the presence of some of the large crest- and toe- clustering patterns, as in Wenchuan along the Subo river, or east of Beichuan. Additional field observations in these areas may help to document these signals.

Our results reconsider the hypothesis of Meunier et al, 2008 since we show that the co-seismic landslide position along hillslopes is strongly modulated by geological features (stratigraphy and bedding) and structures (faults and folds). The ground motion intensity controls the landslide density (Meunier et al., 2007; Yuan et al., 2013), and seems to influence the distribution of the landslide size (Marc et al., 2016, Valagussa et al., 2019), but seems to be a secondary control on their positions along hillslopes in geologically contrasted epicentral areas. Therefore, hazard scenarios for earthquake-induced landslides should not consider only lithology-units but strive to also consider stratigraphic and structural objects that can favor landsliding on specific hillslope sections.

Author contributions

C. Rault has developed the method computed results and prepared the manuscript.

P. Meunier has developed the method, computed results and prepared the manuscript.

A. Robert, has contributed her expertise on geological structures in the Wenchuan earthquake area and prepared the manuscript.

O. Marc has mapped the rainfall-triggered landslides in Taiwan and prepared the manuscript

N. Hovius has participated into of method development and preparation of the manuscript

Competing interests

The authors declare that they have no conflict of interest.

Acknowledgments

295   We thank M. Pubellier for its relevant discussions.

References

Allen, T. I. and Wald, D.: Topographic Slope as a Proxi for Seismic Site-Conditions (VS30) and Amplification Around the Globe., 2007.

Angelier, J., Lee, J. C., Chu, H. T., Hu, J. C., Lu, C. Y., Chan, Y. C., Tin-Jai, L., Font, Y., Deffontaines, B. and Yi-Ben, T.:
300   Le séisme de Chichi (1999) et sa place dans l'orogène de Taiwan, Comptes Rendus de l'Academie de Sciences - Serie IIa: Sciences de la Terre et des Planetes, 333(1), 5–21, doi:10.1016/S1251-8050(01)01563-4, 2001.

Ashford, S. A., Sitar, N., Lysmer, J. and Deng, N.: Topographic effects on the seismic response of steep slopes, Bulletin of the Seismological Society of America, 87(3), 701–709, 1997.

Asimaki, D. and Mohammadi, K.: On the complexity of seismic waves trapped in irregular topographies, Soil Dynamics and
305   Earthquake Engineering, 114(July), 424–437, doi:10.1016/j.soildyn.2018.07.020, 2018.

Boore, D. M.: The effect of simple topography on seismic waves: implications for the accelerations recorded at Pacoima Dam, San Fernando Valley, California, Bulletin of the seismological society of America, 63(5), 1603–1609, 1973.

Burjánek, J., Edwards, B. and Fäh, D.: Empirical evidence of local seismic effects at sites with pronounced topography: A systematic approach, Geophysical Journal International, ggu014, 2014.

310   Camanni, G., Brown, D., Alvarez-Marron, J., Wu, Y.-M. and Chen, H.-A.: The Shuilikeng fault in the central Taiwan mountain belt, Journal of the Geological Society, 171(1), 117–130, doi:10.1144/jgs2013-014, 2014.

Chávez-Garcia, F. J., Sánchez, L. R. and Hatzfeld, D.: Topographic site effects and HVSR. A comparison between observations and theory, Bulletin of the Seismological Society of America, 86(5), 1559–1573, 1996.

Chien, F.C. and Kuo, H.C.: On the extreme rainfall of Typhoon Morakot (2009), Journal of Geophysical Research:
315   Atmospheres, 116, D05104, doi:10.1029/2010JD015092, 2011.

De Michele, M., Raucoules, D., De Sigoyer, J., Pubellier, M. and Chamot-Rooke, N.: Three-dimensional surface displacement of the 2008 May 12 Sichuan earthquake (China) derived from Synthetic Aperture Radar: Evidence for rupture on a blind thrust, Geophysical Journal International, 183(3), 1097–1103, doi:10.1111/j.1365-246X.2010.04807.x, 2010.

Demir, G., Aytekin, M., Akgün, A., Ikizler, S. B. and Tatar, O.: A comparison of landslide susceptibility mapping of the
320   eastern part of the North Anatolian Fault Zone (Turkey) by likelihood-frequency ratio and analytic hierarchy process methods, Natural Hazards, 65(3), 1481–1506, 2013.

Densmore, A. L. and Hovius, N.: Topographic fingerprints of bedrock landslides, Geology, 28(4), 371–374, 2000.

Gallipoli, M. R., Bianca, M., Mucciarelli, M., Parolai, S. and Picozzi, M.: Topographic versus stratigraphic amplification: Mismatch between code provisions and observations during the L'Aquila (Italy, 2009) sequence, Bulletin of Earthquake Engineering, 11(5), 1325–1336, doi:10.1007/s10518-013-9446-3, 2013.

Geli, L., Bard, P.-Y. and Jullien, B.: The effect of topography on earthquake ground motion: a review and new results, Bulletin of the Seismological Society of America, 78(1), 42–63, 1988.

Glinsky, N. and Bertrand, E.: Numerical Investigation of Topographical Site Effects : Parametric Study on Simplified Geometries and Impact of the Inner Geological Structure, , (1909), 2017.

Godard, V., Lavé, J., Carcaillet, J., Cattin, R., Bourlès, D. and Zhu, J.: Spatial distribution of denudation in Eastern Tibet and regressive erosion of plateau margins, Tectonophysics, 491(1–4), 253–274, doi:10.1016/j.tecto.2009.10.026, 2010.

Gorum, T., Fan, X., Van Westen, C. J., Huang, R. Q., Xu, Q., Tang, C. and Wang, G.: Distribution pattern of earthquake-induced landslides triggered by the 12 May 2008 Wenchuan earthquake, Geomorphology, 133(3–4), 152–167, doi:10.1016/j.geomorph.2010.12.030, 2011.

Harp, E. L. and Jibson, R. W.: Landslides triggered by the 1994 Northridge, California, earthquake, Bulletin of the Seismological Society of America, 86(1 SUPPL. B), 1996.

Hartzell, S., Meremonte, M., Ramirez-Guzmán, L. and McNamara, D.: Ground motion in the presence of complex topography: Earthquake and ambient noise sources, Bulletin of the Seismological Society of America, 104(1), 451–466, 2014.

Havenith, H. B., Vanini, M., Jongmans, D. and Faccioli, E.: Initiation of earthquake-induced slope failure: Influence of topographical and other site specific amplification effects, Journal of Seismology, 7(3), 397–412, doi:10.1023/A:1024534105559, 2003.

Jafarzadeh, F., Shahrabi, M. M. and Jahromi, H. F.: On the role of topographic amplification in seismic slope instabilities, Journal of Rock Mechanics and Geotechnical Engineering, 7(2), 163–170, doi:10.1016/j.jrmge.2015.02.009, 2015.

Kaiser, A., Holden, C. and Massey, C.: Determination of site amplification , polarization and topographic effects in the seismic response of the Port Hills following the 2011 Christchurch earthquake, NZSEE Conference, Wellington, New Zealand, (XX), 1–8 [online] Available from: http://www.nzsee.org.nz/db/2013/Poster_10.pdf, 2013.

Keefer, D. K.: Landslides caused by Earthquakes, Geological Society of America, 95, 406–421, 1984.

Korup, O.: Geomorphic implications of fault zone weakening: Slope instability along the alpine fault, South Westland to Fiordland, New Zealand Journal of Geology and Geophysics, 47(2), 257–267, doi:10.1080/00288306.2004.9515052, 2004.

Liao, H. . and Lee, C. T.: Landsides triggered by the Chi-Chi Earthquake, in Proceedings of the 21st Asian Conference on Remote Sensing, vol. 1&2, pp. 383–388., 2000.

Lin, C. W., Chang, W. S., Liu, S. H., Tsai, T. T., Lee, S. P., Tsang, Y. C., Shieh, C. L. and Tseng, C. M.: Landslides triggered by the 7 August 2009 Typhoon Morakot in southern Taiwan, Engineering Geology, 123(1–2), 3–12, doi:10.1016/j.enggeo.2011.06.007, 2011.

Liu-Zeng, J., Wen, L., Oskin, M. and Zeng, L.: Focused modern denudation of the Longmen Shan margin, eastern Tibetan Plateau, Geochemistry, Geophysics, Geosystems, 12(11), 1–21, doi:10.1029/2011GC003652, 2011.

Lovati, S., Bakavoli, M. K. H., Massa, M., Ferretti, G., Pacor, F., Paolucci, R., Haghshenas, E. and Kamalian, M.: Estimation of topographical effects at Narni ridge (Central Italy): Comparisons between experimental results and numerical modelling, Bulletin of Earthquake Engineering, 9(6), 1987–2005, doi:10.1007/s10518-011-9315-x, 2011.

Marc, O., Hovius, N., Meunier, P., Uchida, T. and Hayashi, S.: Transient changes of landslide rates after earthquakes, Geology, 43, 883–886, doi:10.1130/G36961.1, 2015.

Marc, O., Hovius, N., Meunier, P., Gorum, T. and Uchida, T.: A seismologically consistent expression for the total area and volume of earthquake-triggered landsliding, , doi:10.1002/2015JF003732.Received, 2016.

Marc, O., Meunier, P. and Hovius, N.: Prediction of the area affected by earthquake-induced landsliding based on seismological parameters, Natural Hazards and Earth System Sciences, 17(7), 1159–1175, doi:10.5194/nhess-17-1159-2017, 2017.

Marc, O., Stumpf, A., Malet, J. P., Gosset, M., Uchida, T. and Chiang, S. H.: Towards a global database of rainfall-induced landslide inventories: first insights from past and new events, Earth Surface Dynamics Discussions, (March), 1–28, doi:10.5194/esurf-2018-20, 2018.

Massa, M., Lovati, S., D'Alema, E., Ferretti, G. and Bakavoli, M. K. H.: An experimental approach for estimating seismic amplification effects at the top of a ridge, and the implication for ground-motion predictions: The case of Narni, Central Italy, Bulletin of the Seismological Society of America, 100(6), 3020–3034, doi:10.1785/0120090382, 2010.

Massa, M., Barani, S. and Lovati, S.: Overview of topographic effects based on experimental observations: meaning, causes and possible interpretations, Geophysical Journal International, ggu341, 2014.

Massey, C., Della Pasqua, F., Holden, C., Kaiser, A., Richards, L., Wartman, J., McSaveney, M. J., Archibald, G., Yetton, M. and Janku, L.: Rock slope response to strong earthquake shaking, Landslides, 14(1), 249–268, doi:10.1007/s10346-016-0684-8, 2017.

Maufroy, E., Cruz-Atienza, V. M., Cotton, F. and Gaffet, S.: Frequency-Scaled Curvature as a Proxy for Topographic Site-Effect Amplification and Ground-Motion Variability, Bulletin of the seismological society of America, 105(1), 354–367,

2015.

Meunier, P., Hovius, N. and Haines, A. J.: Regional patterns of earthquake-triggered landslides and their relation to ground motion, Geophysical Research Letters, 34(20), 2007.

Meunier, P., Hovius, N. and Haines, J. A.: Topographic site effects and the location of earthquake induced landslides, Earth and Planetary Science Letters, 275(3–4), 221–232, doi:10.1016/j.epsl.2008.07.020, 2008.

MOEA and Central Geological Survey: Geological Map Database, [online] Available from: http://gis.moeacgs.gov.tw/gwh/gsb97-1/sys8/index.cfm (Accessed 12 December 2017), 2008.

Molnar, P.: Interactions among topographically induced elastic stress, static fatigue, and valley incision, Journal of Geophysical Research: Earth Surface, 109(F2), n/a-n/a, doi:10.1029/2003JF000097, 2004.

Ohtsuki, A. and Harumi, K.: Effect of topography and subsurface inhomogeneities on seismic SV waves, Earthquake Engineering & Structural Dynamics, 11(4), 441–462, doi:10.1002/eqe.4290110402, 1983.

Paolucci, R.: Amplification of earthquake ground motion by steep topographic irregularities, Earthquake engineering & structural dynamics, 31(10), 1831–1853, 2002.

Parker, R. N., Densmore, A. L., Rosser, N. J., de Michele, M., Li, Y., Huang, R., Whadcoat, S. and Petley, D. N.: Mass wasting triggered by the 2008 Wenchuan earthquake is greater than orogenic growth, Nature Geoscience, 4, 449 [online] Available from: https://doi.org/10.1038/ngeo1154, 2011

Pedersen, H. A., LeBrun, B., Hatzfeld, D., Campillo, M. and Bard, P. Y.: Ground motion amplitude across ridges, Bull. Seismol. Soc. Am., 84(6), 1786–1800, 1994.

Pilz, M., Parolai, S., Petrovic, B., Silacheva, N., Abakanov, T., Orunbaev, S. and Moldobekov, B.: Basin-edge generated Rayleigh waves in the almaty basin and corresponding consequences for ground motion amplification, Geophysical Journal International, 213(1), 301–316, doi:10.1093/gji/ggx555, 2018.

Poursartip, B. and Kallivokas, L. F.: Model dimensionality effects on the amplification of seismic waves, Soil Dynamics and Earthquake Engineering, 113(September 2017), 572–592, doi:10.1016/j.soildyn.2018.06.012, 2018.

Poursartip, B., Fathi, A. and Kallivokas, L. F.: Seismic wave amplification by topographic features: A parametric study, Soil Dynamics and Earthquake Engineering, 92(July 2016), 503–527, doi:10.1016/j.soildyn.2016.10.031, 2017.

Robert, A.: Déformation polyphasée et importance de l ' héritage structural dans les Longmen Shan (Sichuan , Chine) Apports d ' une approche couplée entre géophysique et géologie, ENS Paris., 2011.

Rodríguez, C. E., Bommer, J. J. and Chandler, R. J.: Earthquake-induced landslides: 1980-1997, Soil Dynamics and Earthquake Engineering, 18(5), 325–346, doi:10.1016/S0267-7261(99)00012-3, 1999.

410   Scheingross, J. S., Minchew, B. M., Mackey, B. H., Simons, M., Lamb, M. P. and Hensley, S.: Fault-zone controls on the spatial distribution of slow-moving landslides, Bulletin of the Geological Society of America, 125(3–4), 473–489, doi:10.1130/B30719.1, 2013.

Sepúlveda, S. A., Serey, A., Lara, M., Pavez, A. and Rebolledo, S.: Landslides induced by the April 2007 Aysén Fjord earthquake, Chilean Patagonia, Landslides, 7(4), 483–492, doi:10.1007/s10346-010-0203-2, 2010.

415   Somerville, P., Saikia, C., Wald, D. and Graves, R.: Implications of the Northridge earthquake for strong ground motions from thrust faults, Bulletin of the Seismological Society of America, 86(1 SUPPL. B), 115–125, 1996.

Stahl, T., Bilderback, E. L., Quigley, M. C., Nobes, D. C. and Massey, C. I.: Coseismic landsliding during the Mw7.1 Darfield (Canterbury) earthquake: Implications for paleoseismic studies of landslides, Geomorphology, 214, 114–127, doi:10.1016/j.geomorph.2014.03.020, 2014.

420   Strand, C. W. J. and R. G.: Geologic Map of California, Los Angeles Sheet, San Francisco, CA, 1969.

Tanyaş, H., Van Westen, C. J., Allstadt, K. E., Jessee, M. A. N., Görüm, T., Jibson, R. W., Godt, J. W., Sato, H. P., Schmitt, R. G., Marc, O. and Hovius, N.: Presentation and Analysis of a Worldwide Database of Earthquake-Induced Landslide Inventories, Journal of Geophysical Research: Earth Surface, 122(10), 1991–2015, doi:10.1002/2017JF004236, 2017.

Tong, X., Sandwell, D. T. and Fialko, Y.: Coseismic slip model of the 2008 Wenchuan earthquake derived from joint
425   inversion of interferometric synthetic aperture radar, GPS, and field data, Journal of Geophysical Research, 115(B4), B04314, doi:10.1029/2009JB006625, 2010.

Tsai, Y. B., & Huang, M. W. (2000). Strong ground motion characteristics of the chichi, Taiwan, earthquake of September 21, 1999. Institute of Geophysics, National Central University.

Tseng, C.M., Chen, Y.R. and Wu, S. M.: Scale and spatial distribution assessment of rainfall-induced landslides along
430   mountain roads, Natural Hazards and Earth System Sciences Discussions, 1–46, doi:10.5194/nhess-2017-264, 2017.

Tu, J. T., Chou, C. and Chu, P. S.: The abrupt shift of typhoon activity in the vicinity of Taiwan and its association with western North Pacific-East Asian climate change, Journal of Climate, 22(13), 3617–3628, doi:10.1175/2009JCLI2411.1, 2009.

U.S. Geological Survey: Earthquake hazard program: ShakeMap, 2018 [online] Available from:
435   https://earthquake.usgs.gov/data/shakemap/ (Accessed 1 January 2018a), 2018a.

U.S. Geological Survey: USGS Geoscience Data Catalog: landslides, [online] Available from: https://geo-nsdi.er.usgs.gov/catalog/combine.php?term=2-639&with=2-700 (Accessed 1 January 2018), 2018b.

Valagussa, A., Marc, O., Frattini, P., and Crosta, G. B.: Seismic and geologic controls on earthquake-induced landslide size,

Earth and Planetary Science Letters, *506*, 268-281, 2019.

440 Wasowski, J., Gaudio, V. Del, Casarano, D., Lollino, P. and Muscillo, S.: Local Scale Seismic Landslide Susceptibility Assessment Based on Historic Earthquake Records Combined with Accelerometer Monitoring and Ambient Noise Data, in Earthquake-Induced Landslides, edited by K. Ugai, H. Yagi, and A. Wakai, pp. 11–20, Springer Berlin Heidelberg, Berlin, Heidelberg., 2013.

Weissel, J.K., and Stark, C. P..: Landslides triggered by the 1999 Mw7. 6 Chi Chi earthquake in Taiwan and their
445 relationship to topography, in Geoscience and Remote Sensing Symposium, vol. 2, pp. 759–761., 2001.

Wen, Z., Xie, J., Gao, M., Hu, Y. and Chau, K. T.: Near-source strong ground motion characteristics of the 2008 Wenchuan earthquake, Bulletin of the Seismological Society of America, 100(5 B), 2425–2439, doi:10.1785/0120090266, 2010.

Winterer, E. L. and Durham, D. L.: Geology of the southeastern Ventura Basin, Los Angeles County, California., 1962.

Xu, C., Xu, X., Yao, X. and Dai, F.: Three (nearly) complete inventories of landslides triggered by the May 12, 2008
450 Wenchuan Mw 7.9 earthquake of China and their spatial distribution statistical analysis, Landslides, 11(3), 441–461, doi:10.1007/s10346-013-0404-6, 2014.

Yerkes, R.F., Campbell, R.H., Alvarez, R.M. and Bovard, K.R.: Preliminary geologic map of the Los Angeles 30′× 60′ Quadrangle, southern California. US Geological Survey Open File Report, 1019, 2005. Chávez-García, F. J., Sánchez, L. R. and Hatzfeld, D.: Topographic site effects and HVSR. A comparison between observations and theory, Bulletin of the
455 Seismological Society of America, 86(5), 1559–1573, 1996.

Yuan, R. M., Deng, Q. H., Cunningham, D., Xu, C., Xu, X. W. and Chang, C. P.: Density distribution of landslides triggered by the 2008 Wenchuan earthquake and their relationships to peak ground acceleration, Bulletin of the Seismological Society of America, 103(4), 2344–2355, doi:10.1785/0120110233, 2013.

Table 1: Details of the inventories used of earthquake- and rainfall-induced landslides

Database	Date	Country	Number of landslides	Surface covered by landslides (km²)	Trigger	Landslides inventory origin	Data and Methods used to map the landslides
Pre-Chi-Chi	1994 - 1999	Taïwan	375	2.7	Rainfall	(Marc et al., 2015)	Satellites images
Chi-Chi	1999	Taïwan	9 272	127.6	Earthquake	(Liao & Lee, 2000)	Aerial photographs and satellites images
Post-Chi-Chi	1999 - 2004	Taïwan	1 647	10.1	Rainfall	(Marc et al., 2015)	Satellites images and air photos
Morakot	2009	Taïwan	17 344	225.0	Typhoon	(Marc et al., 2018)	Satellites images
Wenchuan	2008	China (Sichuan)	197 481	1 160	Earthquake	(Xu et al, 2014)	Aerial photographs and satellites images
Northridge	1999	USA (California)	11 111	25.9	Earthquake	(Harp & Jibson, 1996)	Air photos and field observations
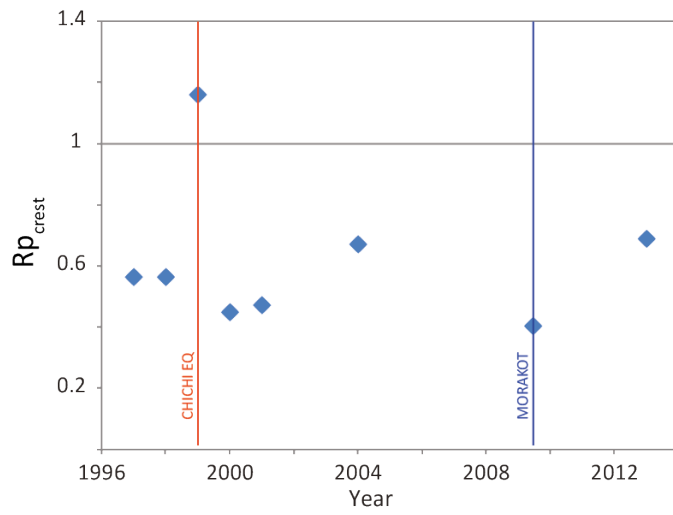
Figure 1: Time variation of the landslide crest-clustering Rp_{crest} in three watersheds in the Chi-Chi epicentral area mapped in Fig.

465 **2. Chi-Chi-induced landslides sit well above the previous and subsequent rainfall-triggered landslides.**
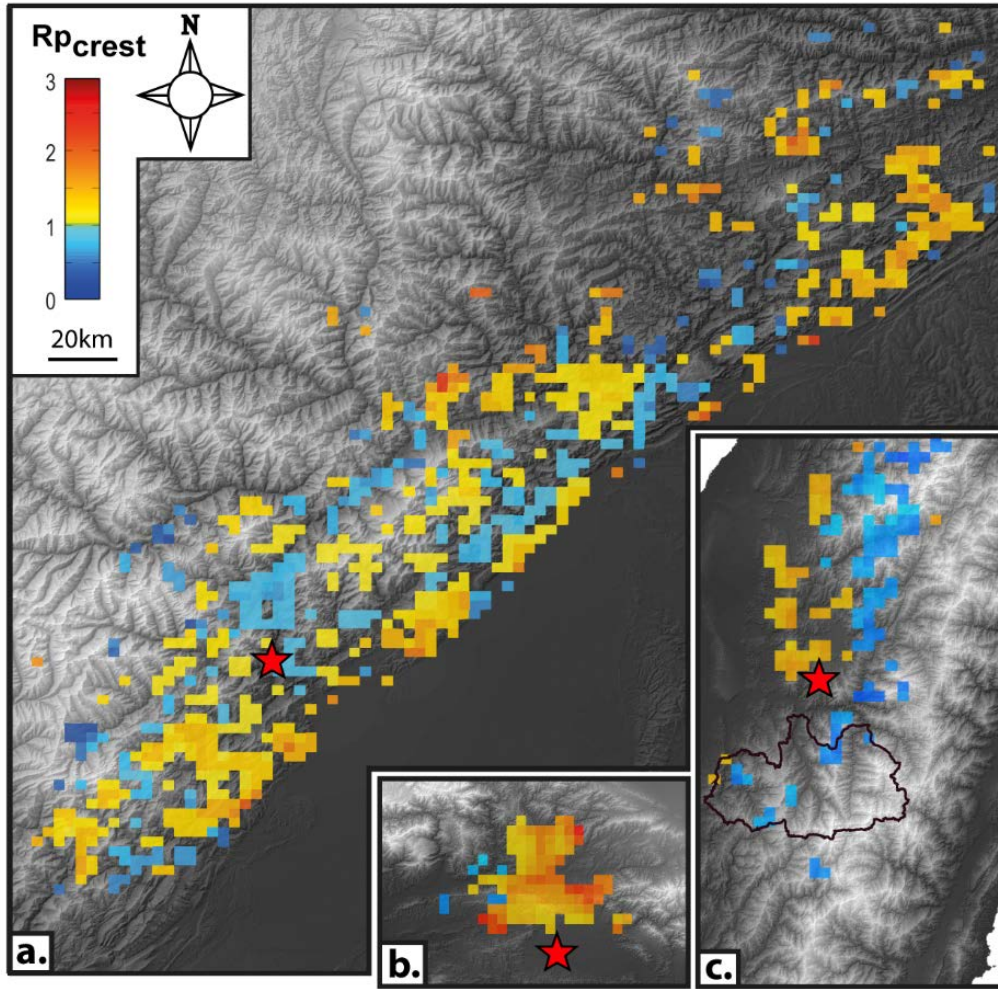
Figure 2: *Rp_{crest}* maps in the a. Wenchuan, b. Northridge and c. Chi-Chi epicentral area. The 3 maps are at the same scale. The study area are divided in macrocells of 7.8km². Only cells of *Rp_{crest}* above the 90% prediction interval are represented (see Methods and Metrics). Regions of crest-clustering are colored in yellow-red. Regions of toe-clustering are colored in blue. Clear coherent patterns of crest- and toe-clustering are identified. The black curve delimits the 3 watersheds where *Rp_{crest}* is documented between 1996 and 2014 (Fig. 1).

470
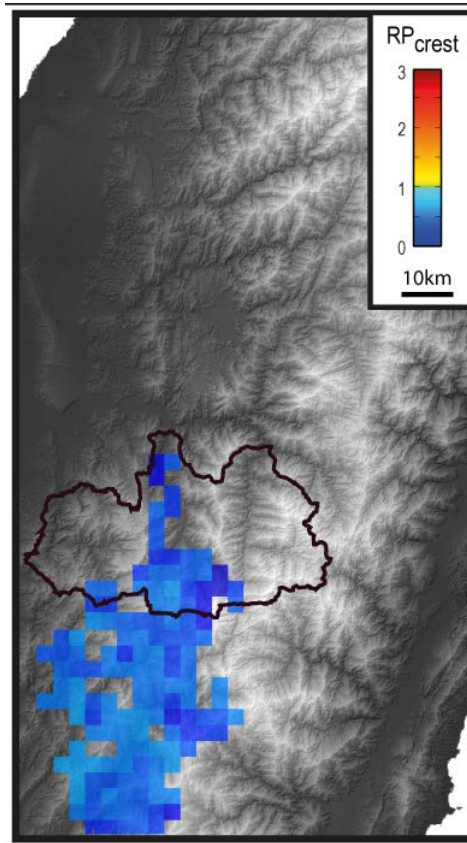
Figure 3: Rp_{crest} map associated with the typhoon Morakot induced landslides in the southern west part of the Chi-Chi epicentral area. Only toe-clustering is observed. The black line delimits the 3 watersheds where Rp_{crest} is documented from 1996 to 2014 for rainfall and Chi-Chi induced landslides (Fig. 1).
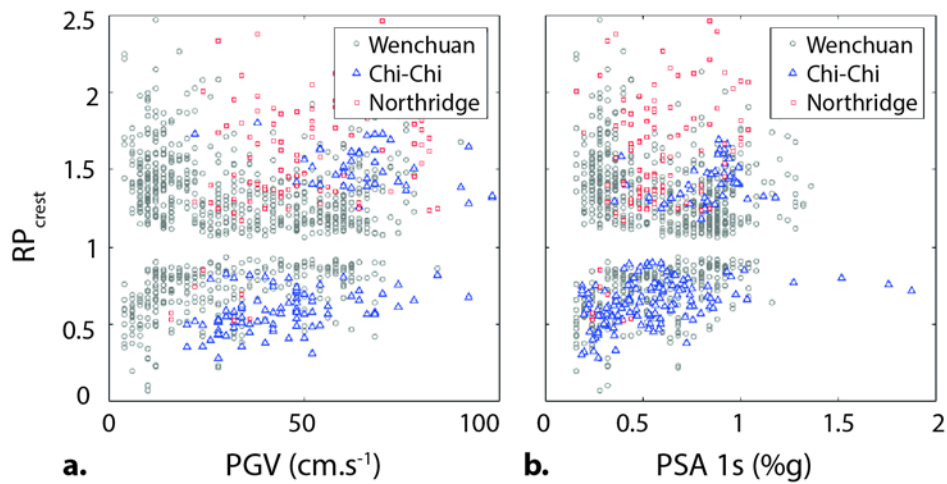
Figure 4: Rp_{crest} **as a function of seismic features: a. Median Peak Ground Velocity (PGV) (m.s^{-1}), b. Median Pseudo Spectral Acceleration at 1s (PSA 1s) calculated in the Wenchuan, Northridge and Chi-Chi epicentral areas. Regional seismic parameters do not seem to explain landslide position along hillslopes.**
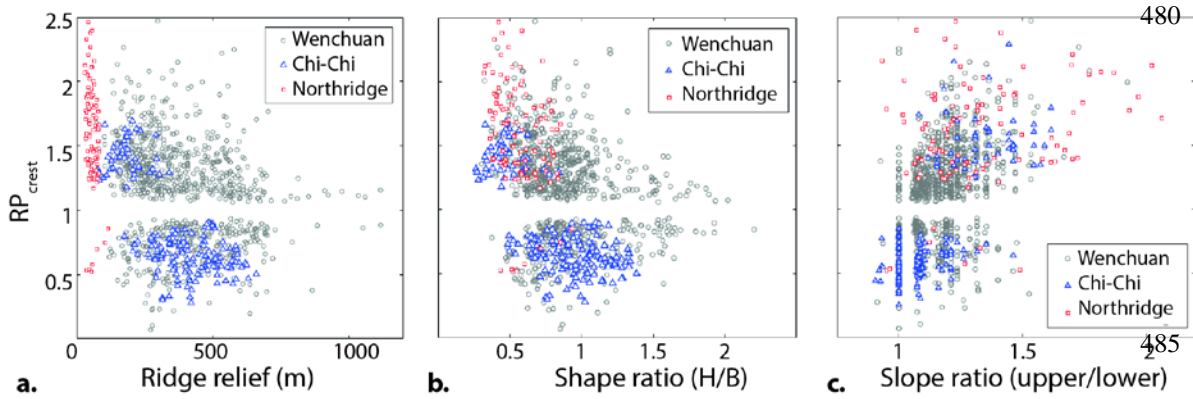
Figure 5: Rp_{crest} **as a function of topographic features: a. ridge relief, b. hill shape ratio (H ridge relief, B half width of the hill) and c. upper over lower hillslope gradient ratio calculated in the Wenchuan, Northridge and Chi-Chi epicentral areas.**
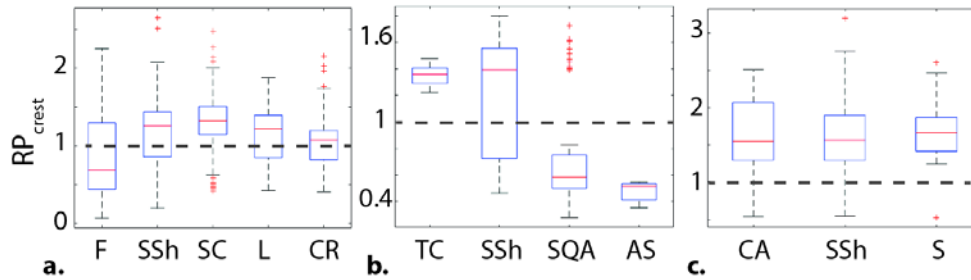
Figure 6: Rp_{crest} **as function of the lithologic groups of the a. Wenchuan, b. Chi-Chi and c. Northridge epicentral areas. F: flysh; SSh: mostly sandstones and shales; SC: mostly sandstones and conglomerates; L: mostly limestones; CR: crystalline rocks; TC: terrace deposits and conglomerates; SQA: shaly sandstones, quartzite and argillite; AS: argillite and sandstones; CA: colluvium and alluvium; S: mostly sandstones.**
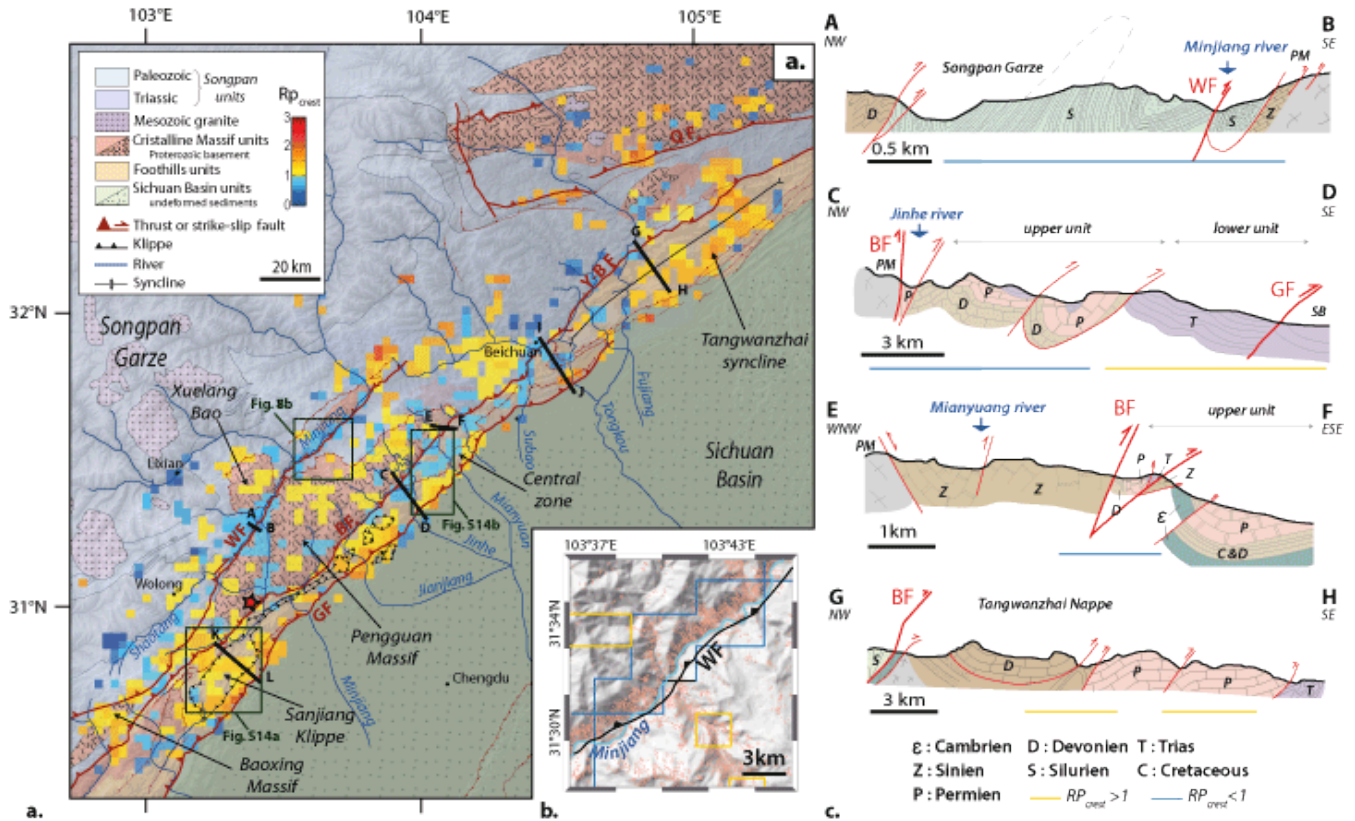
Figure 7: a. Structural map of the Wenchuan earthquake epicentral area (after Robert, 2011) overlaid with the Rp_{crest} map. b. Snapshot of the landslide map in a portion of the Wenchuan shear zone. Its location is reported in Fig. 7.a. Polygons with red contours represent the co-seismic landslides mapped by Xu et al., 2014. The yellow and blue lines delimit zones of crest- and toe- clustering respectively. c. Cross sections of different structural units after Robert 2011. Cross sections I-J and K-L are presented in Fig. S15. Complementary snapshots of the landslide map are shown in Fig. S14. GF: Guanxian fault, BF Beichuan fault, WF Wenchuan fault, Y-B F Yinxiu-Beichuan fault, QF Qinling fault.